Anisotropic Actuation with Piezoelectric Fiber Composites

AARON A. BENT,* NESBITT W. HAGOOD AND JOHN P. RODGERS
Space Engineering Research Center, Massachusetts Institute of Technology, Cambridge, MA 02139

ABSTRACT: An investigation was made into the field of planar structural actuation with anisotropic active materials. The mechanisms for creating anisotropic actuators were discussed, and the impact of anisotropy was shown at the individual lamina level and at the laminated structure level. Models for laminated structures were developed using an augmented Classical Laminated Plate Theory incorporating induced stress terms to accommodate anisotropic actuator materials. A twist-extension coupled laminate was used to exemplify how twist can be directly induced into isotropic host structures using anisotropic actuation. Four anisotropic actuators with different material anisotropies were compared using this example. Finally, a laminate incorporating piezoelectric fiber composite actuators was manufactured and tested. Excellent agreement was found between the predicted and experimental response.

INTRODUCTION

THE field of structural control using active materials has received much attention in recent years. A multitude of models have been developed for the actuation and sensing of beam [1], plate [2], and shell [3] structures employing a variety of active elements. Experimental results in the closed loop control of structural vibration [4], aeroelastic response [5], and acoustic transmission [6] have verified these models and demonstrated the feasibility of active structural control using active materials. As the field has matured, attention has turned toward increasing the performance of these systems. However, the basic active materials have not changed in the past twenty years. Avenues for increasing performance will rely on using current materials in unique ways, or combining materials to create new technologies.

One means of improving the level of structural control performance is the use of tailorable anisotropic actuator materials. Tailoring gives the designer added freedom to specify varying degrees of structural coupling. However, current methods of actuation and sensing that utilize piezoceramics must use monolithic ceramics that exhibit in-plane isotropy. Thus, it is impossible to distinguish and actuate any single component of in-plane strain with these ceramics. Present methods to induce anisotropy require a composite host structure [2], or special piezoelectric attachment techniques [7] to produce the desired degree of coupling.

Piezoelectric fiber composites, however, have a large potential for independently controlling structural deflections in different directions. This arises from the ability to choose parameters at the material, lamina, and laminate levels of manufacture. Matrix and ceramic combinations, volume fractions, and ply angles all contribute to the tailorability of the actuator. As a result, the designer can minimize or maximize various coupling parameters that influence the structural behavior. Various torsional, bending, and extensional modes can now be separated, allowing for more efficient control of independent deflection shapes and the enhancement of control performance.

In some cases, material coupling may be quite beneficial. For example, standard graphite/epoxy materials have been used to modify aeroelastic characteristics of wings. In particular, careful orientation of the fiber direction couples wing-bending and torsional deflections, delaying divergence and increasing lift. Naturally, this technique could be extended to wings incorporating active elements. Ehlers and Weishaar [8] have demonstrated the role of elastic coupling in various aeroelastic structures such as forward and aft swept wings. They report that small amounts of coupling will reduce the actuator strength necessary to increase lift, while enhancing performance by using energy already present in the airstream.

The long term objective of this research is to enable large scale structural control applications by controlling the shape and vibration of composite structures using piezoelectric fiber composite laminae. The modeling and manufacturing of these laminae are the subject of ongoing research with emphasis on developing methods of integration which will result in built-up active structures. The current work quantifies some of the possibilities for anisotropic actuation that are afforded by piezoelectric fiber composites. Thus, this study acts largely as a motivation for development of such composites, and, in addition, seeks to compare various means of anisotropic actuation.

Piezoceramic composites have received a lot of attention in the past fifteen years, particularly in the area of ultrasonic transducers for hydrophones [9] and medical imaging equipment [10]. These transducers have focused primarily on par-

Guest Editor: E. Breitbach.
*Author to whom correspondence should be addressed.

1045-389X/95/03 0338-12 $10.00/0

ticulate composites (0-3 connectivity), and rod composites (1-3 connectivity) with the rods oriented through the thickness of the material. Modeling techniques employed for these composites were an extension of the "Mechanics of Materials" approach to include electrical-mechanical coupling. Piezoelectric Fiber Composites (PFC) differ from the above applications in that they must couple with in-plane structural stresses and strains. As such, the stiff piezoceramic fibers must be oriented in the plane of the structure. The models and manufacturing methods utilized for ultrasonic transducers do not easily carry over to the present form. However, the first paper on PFCs [11] addresses these issues. Techniques borrowed from standard graphite/epoxy composite manufacturing were applied to PZT fiber composites, and a generalized "Uniform Fields" model was developed to provide predictions for effective material properties. The tools are now available to examine various applications of piezoelectric fiber composites.

This paper begins by examining the mechanics involved in modeling anisotropic actuators. The impact of anisotropy at the individual ply level is shown, and the contribution of this anisotropy to the overall laminated structure is modeled using Classical Laminated Plate Theory (CLPT). Four types of anisotropic actuators are introduced and discussed with reference to the different origins of their anisotropy. A special twist-extension coupled laminate example is used to conduct an actuator comparison based on the maximum possible twist for each actuator type. Important concepts relating to induced stress actuators are exemplified through this comparison. Finally, a laminate incorporating PFC actuators is manufactured, tested, and compared to model predictions.

MECHANICS OF AN ANISOTROPIC ACTUATOR

In order to model the active structure and understand the effects of anisotropy, it is first important to properly represent the lamina and laminate properties. Future sections will discuss the properties of particular anisotropic actuators. However, the present discussion will focus on a generic anisotropic actuator. Correct use of the actuator properties will involve manipulations specific to the current problem of planar structural actuation.

Plane Stress Assumptions

Typical applications will include plate and shell structures with and without various substrate materials (aluminum, glass, graphite/epoxy, etc.). In these applications, an important assumption is made about the state of stress in the material. Namely, the normal stress through the thickness and its corresponding shear stresses are zero:

$$T_3 = T_4 = T_5 = 0 \tag{1}$$

This is the common Kirchoff assumption in simple plate and shell theory. To apply this condition, the constitutive equations must be in the compliance form (i.e., with stress as the independent field variable).

The constitutive equations for piezoelectric materials are found in Reference [12], with the standard axis definitions (poling direction coincident with the 3-axis). After reduction, these constitutive equations are

$$\begin{Bmatrix} D_3 \\ S_1 \\ S_2 \\ S_6 \end{Bmatrix} = \begin{bmatrix} \epsilon_{33}^T & d_{31} & d_{32} & 0 \\ d_{31} & s_{11}^E & s_{12}^E & 0 \\ d_{32} & s_{12}^E & s_{22}^E & 0 \\ 0 & 0 & 0 & s_{66}^E \end{bmatrix} \begin{Bmatrix} E_3 \\ T_1 \\ T_2 \\ T_6 \end{Bmatrix} \tag{2}$$

where S_i are the material strains, D_i the electrical displacements, T_i the materials stresses, and E_i the electric fields. Constants s^E and ϵ^T relate the respective elastic and electric fields, while coupling between fields is described by the d constants. Note that all d_{ij} are zero for nonactive materials. Compliances and dielectrics for nonactive materials can be distinguished from those of the active ceramic by their lack of superscripts which otherwise indicate the mechanical and electrical boundary conditions. It is important to note that the material constants shown above are the same as those for the three-dimensional case. The remaining strains S_3, S_4, and S_5 are not necessarily zero, but may be calculated after the primary system is solved. Note that the above form applies to the more general case of anisotropy, both piezoelectrically ($d_{32} \neq d_{31}$) and mechanically ($s_{22}^E \neq s_{11}^E$) than that for monolithic PZT.

In some cases it may be more convenient to represent the piezoelectric properties in a form other than that used to enforce the plane stress assumptions. A common alternate form is

$$\begin{Bmatrix} D_3 \\ T_1 \\ T_2 \\ T_6 \end{Bmatrix} = \begin{bmatrix} \epsilon_{33}^S & e_{31} & e_{32} & 0 \\ -e_{31} & c_{11}^E & c_{12}^E & 0 \\ -e_{32} & c_{12}^E & c_{22}^E & 0 \\ 0 & 0 & 0 & c_{66}^E \end{bmatrix}^* \begin{Bmatrix} E_3 \\ S_1 \\ S_2 \\ S_6 \end{Bmatrix} \tag{3}$$

where e_{ij} are the piezoelectric induced stress constants. This form provides the mechanical stress terms as the dependent variable. Such an expression is useful when modeling the response of a structure to a load applied by an actuator, and will be used in the subsequent sections. A comparison of the two above forms shows:

$$\mathbf{c}^{E*} = (\mathbf{s}^{E*})^{-1} \quad \mathbf{e}^* = \mathbf{d}^*\mathbf{c}^{E*} \quad \boldsymbol{\epsilon}^{S*} = \boldsymbol{\epsilon}^{T*} - \mathbf{d}^*\mathbf{c}^{E*}\mathbf{d}_t^* \tag{4}$$

Since the relations are based on the plane stress assumptions, the above constants (designated with a "*" to show plane stress) will *not* have a one-to-one correspondence to those constants derived from a fully three-dimensional analysis. The relationship between the full three-dimensional

constants to those above are given in the Appendix. From this point on, the inverted properties will be assumed to describe a plane stress situation, and the asterisk symbol will be omitted.

Property Rotations

One possibility for tailoring at the laminate level includes placing the principal actuator axes in directions other than the global structural axes. Since the problem is solved in the global coordinates, it is necessary to rotate the material properties to align with these directions. Consider the in-plane rotation about the 3-axis of a $[+\theta]$ angle laminate from the material axes $(\tilde{1}\text{-}\tilde{2})$ into the global axes (1-2). The relationship between the field variables is:

$$\tilde{\mathbf{D}} = \mathbf{R}_E\mathbf{D} \quad \tilde{\mathbf{E}} = \mathbf{R}_E\mathbf{E} \quad \tilde{\mathbf{S}} = \mathbf{R}_S\mathbf{S} \quad \tilde{\mathbf{T}} = (\mathbf{R}_{S_t})^{-1}\mathbf{T} \tag{5}$$

where subscript t refers to matrix transpose. Rotations of the material properties about the 3-direction can be achieved using first and second order transformation matrices:

$$\mathbf{R}_S = \begin{bmatrix} \cos^2\theta & \sin^2\theta & \cos\theta\sin\theta \\ \sin^2\theta & \cos^2\theta & -\cos\theta\sin\theta \\ -2\cos\theta\sin\theta & 2\cos\theta\sin\theta & \cos^2\theta - \sin^2\theta \end{bmatrix} \tag{6}$$

$$\mathbf{R}_E = \begin{bmatrix} \cos\theta & \sin\theta & 0 \\ -\sin\theta & \cos\theta & 0 \\ 0 & 0 & 1 \end{bmatrix}$$

Simple matrix algebra brings about the rotated material matrix:

$$\begin{bmatrix} \epsilon^S & \mathbf{e} \\ -\mathbf{e}_t & \mathbf{c}^E \end{bmatrix}_{global} = \begin{bmatrix} \mathbf{R}_{E_t}\tilde{\epsilon}^S\mathbf{R}_E & \mathbf{R}_{E_t}\tilde{\mathbf{e}}\mathbf{R}_S \\ -\mathbf{R}_{S_t}\tilde{\mathbf{e}}_t\mathbf{R}_E & \mathbf{R}_{S_t}\tilde{\mathbf{c}}^E\mathbf{R}_S \end{bmatrix} \tag{7}$$

Anisotropy at the Lamina Level

The investigation of anisotropy at the lamina level considers the effects of parameter variations on the single-ply actuator. Anisotropy at this level may be present in the actuator material in two ways:

1. Mechanical anisotropy: shown in the stiffness constants $(\tilde{c}_{22} \neq \tilde{c}_{11})$
2. Piezoelectric anisotropy: shown in the free-strain constants $(\tilde{d}_{32} \neq \tilde{d}_{31})$

The piezoelectric induced stress constant, $\tilde{e}_{ij}$, is an effective measure of anisotropy at the lamina level because it embodies both origins of anisotropy in a single constant:

$$\begin{aligned} \tilde{e}_{31} &= \tilde{c}^E_{11}\tilde{d}_{31} + \tilde{c}^E_{12}\tilde{d}_{32} \\ \tilde{e}_{32} &= \tilde{c}^E_{12}\tilde{d}_{31} + \tilde{c}^E_{22}\tilde{d}_{32} \end{aligned} \tag{8}$$

A large amount of induced stress anisotropy will exist when $\tilde{e}_{31}$ and $\tilde{e}_{32}$ are very different. Another measure of anisotropy becomes apparent if this lamina is rotated so that the principal axes are not coincident with the structural axes. In this case, an additional nonzero piezoelectric term is created:

$$\begin{aligned} \mathbf{e} &= \mathbf{R}_{E_t}\tilde{\mathbf{e}}\mathbf{R}_S \\ e_{31} &= \tilde{e}_{31}\cos^2\theta + \tilde{e}_{32}\sin^2\theta \\ e_{32} &= \tilde{e}_{31}\sin^2\theta + \tilde{e}_{32}\cos^2\theta \\ e_{36} &= \cos\theta\sin\theta(\tilde{e}_{31} - \tilde{e}_{32}) \end{aligned} \tag{9}$$

The extra term, e_{36}, is the piezoelectric induced shear stress term created through a rotation of the lamina. Its existence depends on the presence of anisotropy and the ply angle. This single term can be used to represent all the effects at the ply level that contribute to anisotropic behavior. Thus, maximizing its magnitude maximizes the anisotropy of the lamina. The maximum values are reached at ply angles of $\pm 45°$. This is easily understood since the ply rotation is completely analogous to a Mohr's circle transformation of stresses, where the maximum shear stress is always realized at this angle. Note that $\tilde{e}_{31}$ and $\tilde{e}_{32}$ may have opposite signs. Recent work by Hagood et al. [13] on Interdigitated Electrode piezoceramics (IDE) has shown that this type of free-strain anistropy is possible.

Anisotropy at the Laminate Level

The ultimate objective for piezoelectric fiber composites is their introduction into a laminated, built-up active structure for control. Thus, it will be important for design purposes to predict overall structural properties and response to various loading conditions. Classical Laminated Plate Theory lends itself well to design studies of laminated structures, and has already proven its value when augmented with actuator-induced forces and moments to extend the analysis to active structures [2,3]. A caveat of the theory is its limitation to a local description of the plate behavior. That is, it does not capture variations in loading or structural geometry within the plane of the structure. Nonetheless, it *is* able to provide accurate predictions of macroscopic deformations for several important cases, and allows for the examination of important laminated structure parameters.

A typical laminated plate section is shown in Figure 1. Axes coincident with those described in the previous section are maintained. Possible loading conditions include edge moments M_1, M_2, and M_6, and in-plane forces N_1, N_2, and N_6. The underlying assumption of this theory is the manner in which the deformations of the typical section are characterized. The remaining Kirchoff assumptions for plate structures, which closely parallel the Bernoulli-Euler derivation

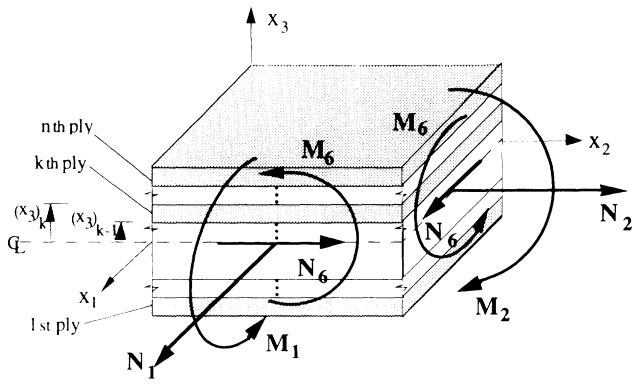

Figure 1. *Classical laminated plate theory definitions.*

for beams [14] are the following: strains are continuous between plies, and plane sections remain perpendicular to the midplane after deformation. The latter assumption is equivalent to requiring that the out-of-plane shear strains (S_4, S_5) be zero, i.e., there is no shear deformation and hence only pure bending or extension. The result of such assumptions is to allow the laminate to be treated as a single material, whose properties are based on some collection of the individual ply properties. Thus, the problem is actually the formulation of the laminate constitutive equations, where kinematic quantities are related to force quantities, given certain assumptions about the strain deformation fields. Given the above assumptions, the assumed strain field may be represented by midplane extensional strains and a curvature strain:

$$S_i = S_i^o + x_3 \boldsymbol{\kappa}_i \quad (i = 1,2,6) \tag{10}$$

where the superscript o denotes displacements of the midplane.

Formulation of the laminate constitutive relations is approached by taking a summation of through the thickness stresss to form global force and moment resultants (from Reference [14]),

$$N_i = \int_{-h/2}^{h/2} (T_i) dx_3 \quad M_i = \int_{-h/2}^{h/2} (T_i x_3) dx_3 \quad (i = 1,2,6) \tag{11}$$

where h refers to the laminate thickness.

Substituting for stresses using the constitutive relations (3), replacing the material strains by the assumed strain fields, Equation (10), and performing the integration in a piecewise manner yields the governing equations:

$$\begin{aligned} \mathbf{N} &= -\mathbf{N}^A + [\mathbf{A}]\mathbf{S}^o + [\mathbf{B}]\boldsymbol{\kappa} \\ \mathbf{M} &= -\mathbf{M}^A + [\mathbf{B}]\mathbf{S}^o + [\mathbf{D}]\boldsymbol{\kappa} \end{aligned} \tag{12}$$

where $\mathbf{N}^A$ and $\mathbf{M}^A$ represent the actuator induced forces and moments. The stiffness terms are

$$\begin{aligned} [\mathbf{A}] &= \sum_{k=1}^{n} (\mathbf{c}^E)_k ((x_3)_k - (x_3)_{k-1}) \\ [\mathbf{B}] &= \frac{1}{2} \sum_{k=1}^{n} (\mathbf{c}^E)_k ((x_3)_k^2 - (x_3)_{k-1}^2) \\ [\mathbf{D}] &= \frac{1}{3} \sum_{k=1}^{n} (\mathbf{c}^E)_k ((x_3)_k^3 - (x_3)_{k-1}^3) \end{aligned} \tag{13}$$

and the actuator induced forces and moments are

$$\begin{aligned} \mathbf{N}^A &= \sum_{k=1}^{n_A} (\mathbf{e}_t E_3)_k ((x_3)_k - (x_3)_{k-1}) \\ \mathbf{M}^A &= \frac{1}{2} \sum_{k=1}^{n_A} (\mathbf{e}_t E_3)_k ((x_3)_k^2 - (x_3)_{k-1}^2) \end{aligned} \tag{14}$$

The number of total laminates is n, and the number of active laminates is n_A. Use of Equations (12) requires knowledge of two of the three possible loading cases (either mechanical forces, total strains, or actuator forces). The loading conditions easiest to implement from a practical standpoint are those of a free[1] expansion where the resultant mechanical loads are zero, and the field voltage applied to the actuators is known. In such a case, Equations (12) can be inverted to solve for the resulting strains and curvatures, which are easily measured through conventional methods.

$$\begin{Bmatrix} \mathbf{S}^o \\ \boldsymbol{\kappa} \end{Bmatrix} = \begin{bmatrix} \mathbf{A} & \mathbf{B} \\ \mathbf{B} & \mathbf{D} \end{bmatrix}^{-1} \begin{Bmatrix} \mathbf{N}^A \\ \mathbf{M}^A \end{Bmatrix} \tag{15}$$

Solution for the midplane strains and curvature strains will provide information on the global laminate deformations. Such information can be used to examine the twist, extension, and bending that can be obtained for an applied electric field and particular structural parameters.

TWIST-EXTENSION COUPLED LAMINATE EXAMPLE

A simple laminate case has been chosen for the purpose of comparing the various actuators. Absolute conclusions on the actuator types cannot be drawn from any one case,

[1]"Free" in the sense of no net applied mechanical loading. Actuator is not undergoing free strain.

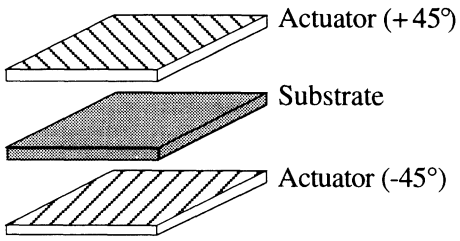

Figure 2. *Laminated structure example.*

because the performance is application-dependent. However, the analysis of this case does provide excellent insight into the fundamentals of anisotropic actuation, allowing easier application to other laminates and loading cases.

The laminate chosen for this study is $[45_A/0_S/-45_A]$, an antisymmetric angle-ply laminate, shown in Figure 2. For positive actuation on both active laminae (i.e., applied electric field coincident with poling direction), the result will be a coupled extension and twist deformation. A $\pm 45°$ angle was chosen to maximize the piezoelectric stress constant e_{36}. An extension-twist coupled laminate is also amenable to experimental verification. Since no bending takes place, the effect of clamping at one end will have little effect on the actuation, and the CLPT model can be used to predict the twist while neglecting end effects.

Analysis

Calculation of the A, B, and D matrices shows a form typical of antisymmetric angle-ply laminates:

$$\begin{Bmatrix} N_1^A \\ N_2^A \\ N_6^A \\ M_1^A \\ M_2^A \\ M_6^A \end{Bmatrix} = \begin{bmatrix} A_{11} & A_{12} & 0 & 0 & 0 & B_{16} \\ A_{12} & A_{22} & 0 & 0 & 0 & B_{26} \\ 0 & 0 & A_{66} & B_{16} & B_{26} & 0 \\ 0 & 0 & B_{16} & D_{11} & D_{12} & 0 \\ 0 & 0 & B_{26} & D_{12} & D_{22} & 0 \\ B_{16} & B_{26} & 0 & 0 & 0 & D_{66} \end{bmatrix} \begin{Bmatrix} S_1^o \\ S_2^o \\ S_6^o \\ \varkappa_1 \\ \varkappa_2 \\ \varkappa_6 \end{Bmatrix} \tag{16}$$

This matrix identifies the coupling present between various deformation modes and represents the *passive* properties of the laminate. Thus, these parameters are independent of mechanical or actuator imposed loads. The above matrix shows that coupling does indeed exist between extension loads $\{N_1, N_2\}$ and twist curvature $\{\varkappa_6\}$, due to the B terms. These terms also couple shear loads $\{N_6\}$ and bending curvatures $\{\varkappa_1, \varkappa_2\}$.

The mechanical loads may be applied completely independently of the material properties of the laminate chosen, implying that any loading combination $\{N_i, M_i\}$ is valid. However, actuator induced loads $\{N_i^A, M_i^A \mid$ are dependent on the material configuration chosen for the laminate, for it is the very lay-up used that determines the possible induced moments and forces. For this particular case with positive actuation on each actuator,

$$N_6^A = M_1^A = M_2^A = 0 \tag{17}$$

These induced loads are zero because the antisymmetric nature of this laminate balances the induced shear forces and applied bending moments. The remaining loads and deformations may be shown as the reduced system:

$$\begin{Bmatrix} N_1^A \\ N_2^A \\ M_6^A \end{Bmatrix} = \begin{bmatrix} A_{11} & A_{12} & B_{16} \\ A_{12} & A_{22} & B_{26} \\ B_{16} & B_{26} & D_{66} \end{bmatrix} \begin{Bmatrix} S_1^o \\ S_2^o \\ \varkappa_6 \end{Bmatrix} \tag{18}$$

Since the antisymmetric ply angle chosen is $\pm 45°$, several additional geometrical symmetries exist. Positive actuation on both actuators also results in symmetry of actuator induced forces:

$$A_{11} = A_{22} \quad B_{16} = B_{26} \quad N_1^A = N_2^A \tag{19}$$

Inverting the above relations (18) and solving for the twist curvature yields:

$$\varkappa_6 = \frac{-2B_{16}N_1^A + (A_{11} + A_{12})M_6^A}{-2B_{16}^2 + D_{66}(A_{11} + A_{12})} \tag{20}$$

where the following geometric and actuator terms are given with the plane stress material constants expressed in the local (ply) coordinates:

$$\begin{aligned} A_{11} + A_{12} &= (t_s(\tilde{c}_{11} + \tilde{c}_{12}) + t_A(\tilde{c}_{11}^E + 2\tilde{c}_{12}^E + \tilde{c}_{22}^E)) \\ B_{16} &= \frac{1}{4}(\tilde{c}_{11}^E - \tilde{c}_{22}^E)(t_A t_S + t_A^2) \\ D_{66} &= \frac{1}{4}\left((\tilde{c}_{11}^E - 2\tilde{c}_{12}^E + \tilde{c}_{22}^E)\left(\frac{t_A t_S^2}{2} + t_A^2 t_S + \frac{2t_A^3}{3}\right) \right. \\ &\quad \left. + \frac{t_S^3}{6}(\tilde{c}_{11} - \tilde{c}_{12})\right) \\ N_1^A &= E_3 t_A(\tilde{e}_{31} + \tilde{e}_{32}) \\ M_6^A &= \frac{1}{2}E_3(\tilde{e}_{31} - \tilde{e}_{32})(t_A t_S + t_A^2) \end{aligned} \tag{21}$$

It is easy to see the important terms that contribute to the twist curvature, $\varkappa_6$. The twist moment, M_6 directly induces twist and is dependent on the existence of piezoelectric stress anisotropy ($\tilde{e}_{31} \neq \tilde{e}_{32}$), as discussed in the section on anisotropy at the lamina level. If stiffness isotropy existed ($\tilde{c}_{11}^E = \tilde{c}_{22}^E$), the term B_{16} would be zero, and the twist would simply be a function of M_6^A and D_{66}. Instead, twist can also be generated by the actuator induced extensional force N_1^A because it is coupled through the B_{16} term. This term does not depend on piezoelectric induced-stress anisotropy, but requires stiffness anisotropy in order to exist.

It is important to note that these constants cannot be independently specified and that c_{ij}^E and e_{ij} are interrelated. For this reason, it is difficult to draw conclusions about the contributions of the individual terms when both effects are present. Thus, actuation will be compared on the basis of stiffness, c_{ij}^E, and piezoelectric free-strain constants, d_{ij}. These constants are also easier to measure, and the free-strain d-constants are a better understood quantity. However, the concept of induced stress remains essential in the discussion of actuators, and will be dealt with further.

Replacing the e_{ij} constants with those from Equation (8), and nondimensionalizing with respect to actuator quantities yields an expression for nondimensional twist curvature:

$$\frac{\varkappa_6 t_A}{\Lambda_{MON}} = \frac{\Lambda_{ACT}}{\Lambda_{MON}} \times [(T + 1)(4R_c(1 - R_d)(1 - R_c\nu_{12_A}^2) + 2T\psi(1 + \nu_{12})(C_B - R_c(1 - \nu_{12_A})(1 + R_d)))] \times \left[-(T + 1)^2(1 - R_c)^2 + 2(C_E + T\psi(1 + \nu_{12})) \times \left(C_B\left(\frac{T^2}{2} + T + \frac{2}{3}\right) + T^3\psi\frac{(1 - \nu_{12})}{6}\right)\right]^{-1} \tag{22}$$

where the nondimensionalized ratios are defined as

$$T = \frac{t_S}{t_A}, \quad \psi = \frac{\tilde{c}_{11}}{\tilde{c}_{11}^E} \quad R_c = \frac{\tilde{c}_{22}^E}{\tilde{c}_{11}^E} \quad R_d = \frac{\tilde{d}_{32}}{\tilde{d}_{31}} \quad \Lambda = \tilde{d}_{31}E_3 \tag{23}$$

$$C_E = 2R_c\nu_{12_A} + R_c + 1 \quad C_B = -2R_c\nu_{12_A} + R_c + 1$$

The terms R_c and R_d are the ratios of transverse to longitudinal properties in the actuator, for stiffness and piezoelectric free strain, respectively. T is the ratio of substrate thickness (t_S) to actuator thickness (t_A), while ψ provides information on the relative stiffness of the actuator and substrate materials. Quantities C_B and C_E are the nondimensional stiffness terms derived from the bending (D_{66}) and extensional ($A_{11} + A_{12}$) groups in the original Equation (20). It is important to note the significance of the Λ terms. Λ is the commonly used free-strain actuation term ($\tilde{d}_{31}E_3$), where Λ_{MON} refers to the actuation capability of a monolithic piezoceramic. The term Λ_{ACT} takes into account the possibility that a particular actuator may have a different free-strain actuation capability than a monolithic piece of the same material (PZT type). One such case is the interdigitated electrode piezoceramics where the poling direction is actually along the geometric 1-axis used here.

Investigating the effects of anisotropy on the twist can be done by varying one parameter, while the others are held constant. In particular, the effect of the stiffness and piezoelectric anisotropy ratios on the twist curvature will be shown as a function of thickness ratio (T). The laminae stiffness ratio (ψ), will be assumed to have the value of one. Stiffer substrate materials will only slightly increase the curvature twist. For the most part, the larger induced actuator stresses will be offset by the larger geometric terms (B_{16}, D_{66}, etc.).

Figure 3 examines the effect of free-strain anisotropy on the nondimensionalized twist curvature. In general, larger free-strain anisotropy enhances the twist. The exception is the case of ideal stiffness anisotropy ($R_c = 0$). This curve shows that if the transverse stiffness is zero, it is impossible to induce any transverse actuator stress loads ($\tilde{e}_{32} = 0$), and thus, the twist is independent of $\tilde{d}_{32}$ and R_d. Therefore, a fundamental limit on actuation potential exists for actuators with high levels of stiffness anisotropy. Furthermore, without a substrate material, the twist caused by the extensional induced loads ($2B_{16}N_1^A$) exactly cancels the twist caused by the twist moment term ($(A_{11} + A_{22})M_6^A$) in the numerator of Equation (20).

The four graphs in Figure 3(a–d) show the progression of twist for decreasing levels of stiffness anisotropy. The last graph is the special case of stiffness isotropy $R_c = 1$. For this special case:

$$\frac{\varkappa_6 t_A}{\Lambda_{MON}} = \frac{\Lambda_{ACT}}{\Lambda_{MON}} \times [(T + 1)(1 - R_d)(1 - \nu_{12_A})] \times \left[(1 - \nu_{12_A})\left(T^2 + 2T + \frac{4}{3}\right) + \frac{\psi T^3(1 - \nu_{12})}{6}\right]^{-1} \tag{24}$$

Interdigitated piezoceramics (IDE) are an example of this special case. Note that the substrate with optimal thickness is actually no substrate at all. The stiffness of the system increases in a cubic manner with substrate thickness, while actuation authority increases only linearly with thickness (increasing the moment arm). Since the actuators in this special case have adequate transverse stiffness ($R_c = 1$), they need not rely on the substrate to provide stiffness for inducing stress. Instead, each actuator pushes against the transverse stiffness of the opposing actuator.

Figure 4 examines the effect of stiffness anisotropy on the curvature twist at various levels of piezoelectric free-strain anisotropy. As expected, for a particular free-strain anisotropy, increasing levels of stiffness anisotropy enhance the twist. For very high levels of free-strain anisotropy ($R_d = -0.5$), this enhancement is small, and is similar to the discussion above, for the case when $R_c = 0$.

The four graphs in Figure 4(a–d) show the progression of twist for decreasing levels of free-strain anisotropy. The last graph is the special case of Equation (22) for $R_d = 1$ (free-strain isotropy):

$$\frac{\varkappa_6 t_A}{\Lambda_{MON}} = \frac{\Lambda_{ACT}}{\Lambda_{MON}} \times [2T\psi(T + 1)(1 + \nu_{12})(1 - R_c)]$$

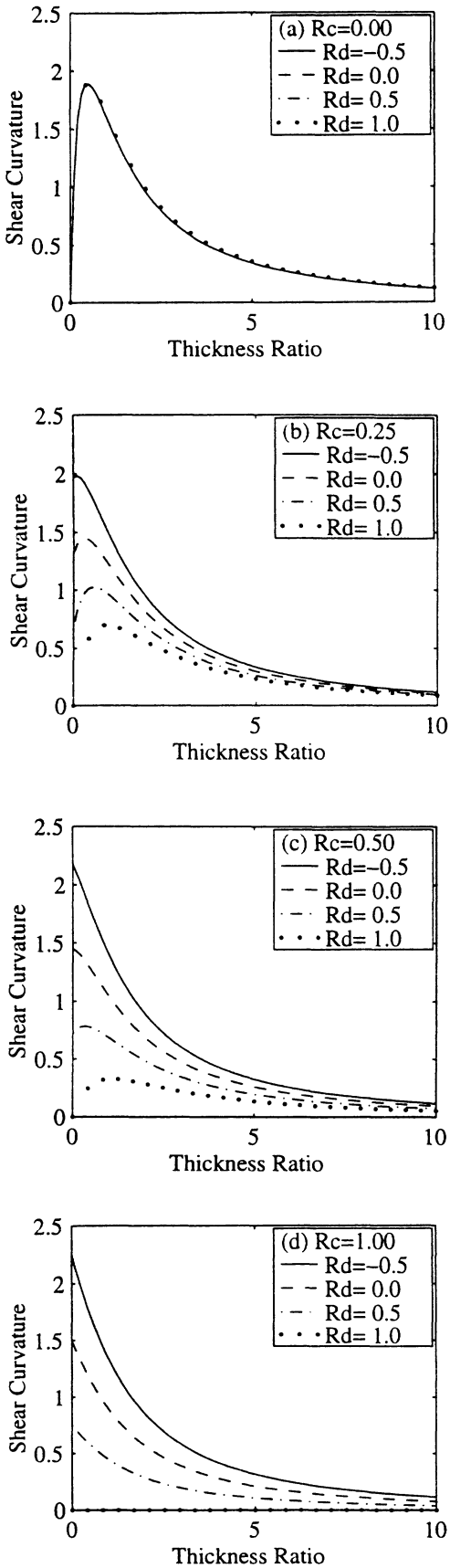

Figure 3. *Nondimensionalized shear curvature for an actuator with free-strain anisotropy, for various stiffness ratios.*

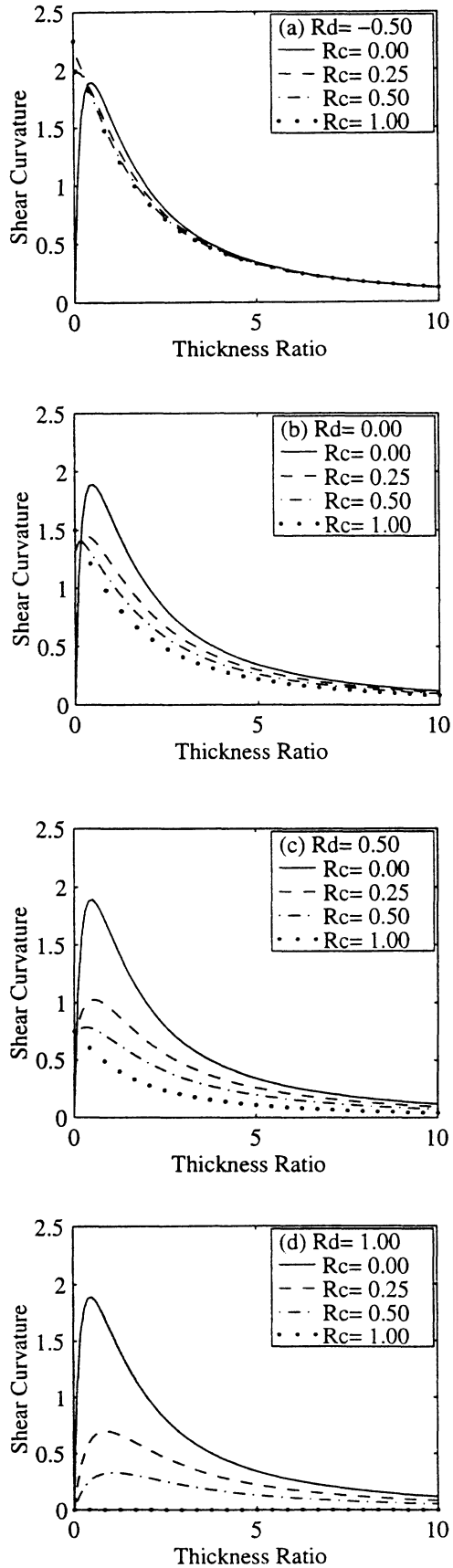

Figure 4. *Nondimensionalized shear curvature for an actuator with stiffness anisotropy, for various free-strain ratios.*

$$\times \left[-(T+1)^2(1-R_c)^2 + 2(C_E + T\psi(1+\vartheta_{12})) \times \left(C_B\left(\frac{T^2}{2} + T + \frac{2}{3}\right) + T^3\psi\frac{(1-\nu_{12_A})}{6}\right)\right]^{-1} \tag{25}$$

Directionally Attached Piezoceramics [7] are an example of actuators employing stiffness anisotropy with isotropic piezoelectric free strain. An interesting aspect of this special case is again the reliance of twist on the presence of a substrate material. For the special case of no substrate ($t_S = 0$) and stiffness anisotropy only ($R_d = 1$), the two numerator terms in Equation (20) again exactly cancel one another. This effect is echoed in Equation (25) for $T = 0$. Thus, there is an optimal substrate thickness for an anisotropically stiff laminate having isotropic free-strain actuation.

ANISOTROPIC ACTUATORS

Up to this point, discussion has been limited to the examination of generic actuators, and the effect of stiffness and free-strain anisotropy on laminated structure actuation. Several different types of anisotropic actuators based on piezoceramic material exist, and have already been referred to throughout the paper. This next section details the attributes of each of these actuators. The purpose is to facilitate a comparison of the fundamental differences in the types of available actuators. The understanding from such a comparison can then be extended to other cases of actuation and laminates.

Piezoelectric Fiber Composites

Piezoelectric fiber composites as a means for anisotropic structural actuation were first introduced by Hagood and Bent [11] in a form that reduces many of the problems inherent in monolithic piezoceramic actuators. The general approach to the proposed concept of built-up active structures is shown in Figure 5. The objective is to produce

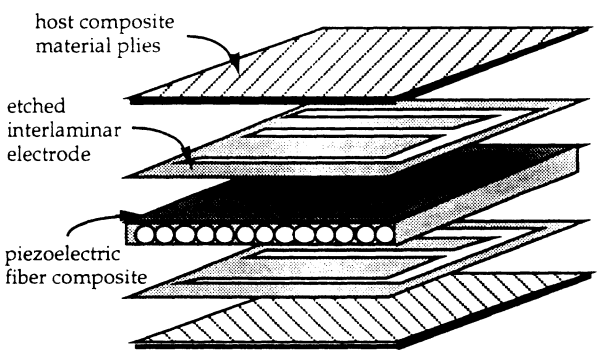

Figure 5. *General approach to built-up active composite structures.*

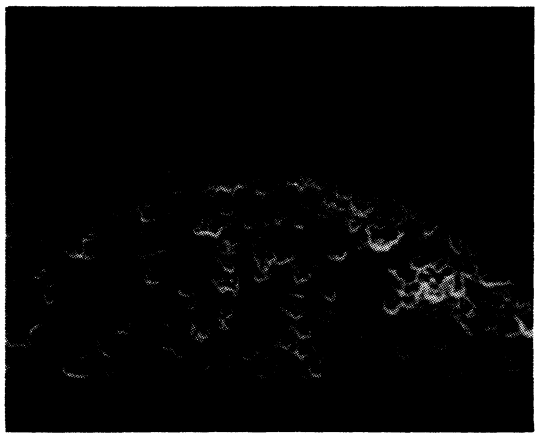

Figure 6. *SEM photograph of piezoelectric fiber composite.*

PFC laminae which can be incorporated between regular graphite/epoxy plies. An electric field would be delivered to the active composite using interlaminar electrodes, which also serve as insulators from the conductive graphite material. The current approach uses conventional electrodes so that the poling direction is through the thickness of the active subply.

The above paper details methods for the modeling and manufacturing of PZT fiber composites. A Uniform Fields approach to micro electromechanical modeling produced effective material constants for the two-phase composite. Manufacturing followed techniques borrowed from well-developed graphite/epoxy cure methods. An SEM photograph (Figure 6) shows some of the more recent techniques in PFC manufacturing. A 120 micron piezoelectric fiber[2] is shown embedded in a soft, epoxy[3] matrix to which PZT particulate[4] has been added to reduce the dielectric mismatch between the two materials. The addition of 75 weight percent of PZT powder (28 volume percent) increases the effective matrix dielectric by a factor of 4.5 (from 6 to ~27). A chemical dispersant[5] further improved the dielectric and reduced the brittleness that would otherwise accompany particulate loading.

Three types of interlaminar electrodes have also been investigated. One type, shown in the photograph, is 0.0005 inch Kapton with a 2500 Å layer of sputtered copper which is bonded onto the active subply at the time of cure. This material is easily etched and has the potential for use as a patterned electrode. The second type involves manufacturing the PFCs without electrodes, lightly sanding to increase surface roughness, and depositing a 3000 Å aluminum layer on each surface through a thermal-vapor deposition process. The third type is similar, except that air-dried silver paint is applied by hand. The present study employs this method of electroding.

[2]CeraNova Corporation, 14 Menfi Way, Hopedale, MA 10747.
[3]Epo-Tek 301 epoxy, Epoxy Technologies, 14 Fortune Dr., Billerica, MA 01821.
[4]PZT 5H-128B, Morgan-Matroc Inc., 232 Forbes Road, Bedford, OH 44146.
[5]Hypermer KD-2, ICI Americas Inc., Wilmington, DE 19897.

Table 1. Plane stress material properties.

	s^E_{11}	s^E_{12}	s^E_{22}	s^E_{66}	c^E_{11}	c^E_{12}	c^E_{22}	c^E_{66}	d_{31}	d_{32}	e_{31}	e_{32}	$\frac{\epsilon^T_{33}}{\epsilon_o}$	$\frac{\epsilon^S_{33}}{\epsilon_o}$
Fibers	16.5	−4.78	16.5	42.6	66.2	19.2	66.2	23.5	−274	−274	−23.4	−23.4	3400	1950
Matrix	294	−88.2	294	764	3.74	1.12	3.74	1.31	0	0	0	0	27.3	27.3

Units: s^E_{ij}: 10^{-12}m²/N, c^E_{ij}: 10^9 N/m², d_{ij}: 10^{-12} m/V, e_{ij}: N/Vm.

For the present comparison, the properties used are those of the current material systems and manufacturing capabilities. Bulk piezoelectric properties for 5H-type PZT are used for the fibers, and the measured properties are used for the particulate-loaded epoxy. These are given in Table 1. The closed form *Uniform Fields* model presented in Reference [11] is used to generate predictions for the actuator parameters. The maximum through-thickness line fraction (X_3) that has been experimentally achieved is 0.98. The width line fraction (X_2) is a free parameter that may be chosen to tailor the composite properties. Figure 7 shows the model predictions for R_d and R_c for a range of X_2 based on the properties given. Nondimensional twist curvature is also shown for a constant thickness ratio of 0.5. This serves only to illustrate the general trend with X_2. An X_2 of 0.5 (equal spacing of fibers and matrix across the width) provides high anisotropy and stiffness, and is chosen for the comparison. In this case, the composite piezoelectric free-strain and stiffness anisotropies are 0.52 and 0.18, respectively. Actuation capability of the PFC actuators is taken to be that of monolithic piezoceramics, as the maximum free strain level in the fiber direction is not changed[6] ($\Lambda_{ACT} = \Lambda_{MON}$).

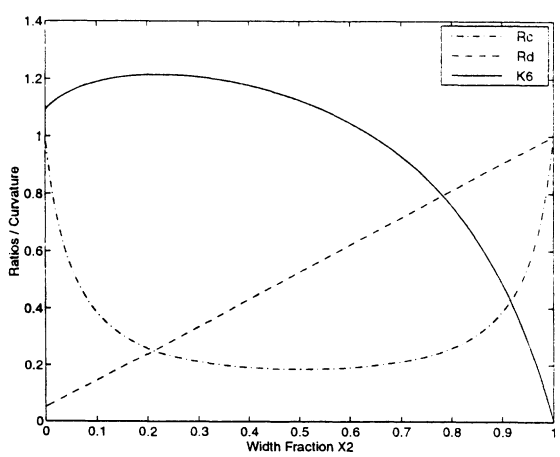

Figure 7. *PFC design curves of anisotropy ratio and nondimensionalized curvature (for T = 0.5).*

[6] d_{31} is not the same as that for monolithic ceramic, but the same level of free strain may be reached by applying higher field levels. Thus Λ is the same as that for monolithic ceramic.

Other Anisotropic Actuators

An Interdigitated Electrode (IDE) piezoceramic directed toward structural actuation was introduced by Hagood et al. [13]. As shown in Figure 8, this novel electrode pattern is composed of electrode fingers with alternating polarities, on both sides of the piezoceramic. As a result, the majority of electric field components are actually in the plane of the actuator, so that poling is in-plane, rather than through the thickness. This creates a high level of free-strain anisotropy because the two free-strain piezoelectric constants are of opposite sign. The model predicts a free-strain anisotropy ratio of $R_d = -0.5$, although experimentally, much higher values were seen due to material nonlinearities and electric field geometric effects. Not only is high anisotropy caused by this electrode pattern, but the in-plane polarization also increases the actuation capability to 1.8 times that of the monolithic piezoceramic ($\Lambda_{ACT} = 1.8\Lambda_{MON}$). However, these actuators have nearly isotropic stiffness ($R_c \approx 1$).

The introduction of Directionally Attached Piezoceramics (DAP) is attributed to Barrett [7]. The concept, shown in Figure 8, incorporates monolithic piezoceramic actuators bonded in special attachment patterns. The bond pattern is typically along a thin line, creating high longitudinal stiffness, but very low transverse stiffness. Barrett reports large levels of stiffness anisotropy (as large as 1/50 to 1/80), but has been limited by practical constraints to values of R_c between 1/7 and 1/20. A value of 1/20 is assumed for the comparison. Since the free-strain piezoelectric constants remain the same in the two directions, the DAP elements are actuators that can be thought of as demonstrating stiffness anisotropy only. The actuation capability of the DAP element is that of the monolithic piezoceramic ($\Lambda_{ACT} = \Lambda_{MON}$).

To complete the comparison of actuators, a hypothetical Unidirectional Actuator (UDA) is proposed. This actuator

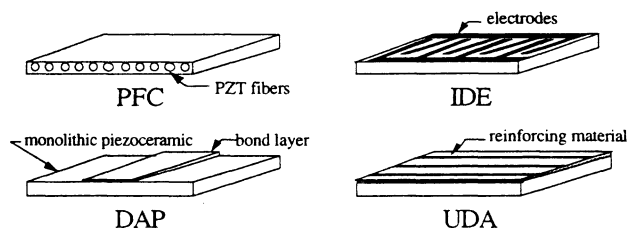

Figure 8. *Anisotropic actuators compared in this analysis.*

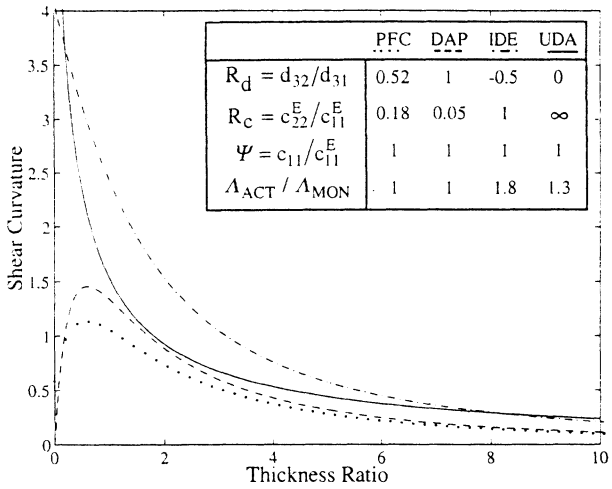

Figure 9. *Comparison of nondimensionalized curvature vs. thickness ratio for four actuators.*

is comprised of a monolithic piezoceramic bonded to an ideal, anisotropically stiff reinforcement material. As an example, this reinforcement material could be composed of extremely stiff fibers embedded in a very soft matrix. The limiting case would be an actuator with an infinite transverse stiffness, giving a stiffness ratio (R_c) of infinity. In addition to creating high stiffness anisotropy, the actuation in the transverse direction would be zero, making the free-strain ratio (R_d) zero. The transverse clamping effect also serves to enhance the longitudinal free-strain piezoelectric constant ($\tilde{d}_{31}$) by a Poisson's term, so that the actuation capability of the UDA is approximately 1.3 times that of a monolithic piezoceramic ($\Lambda_{ACT} = 1.3\Lambda_{MON}$).

Comparison

It is now possible to compare the various actuator types for this antisymmetric laminate case. Comparison is made on the basis of similar substrate materials ($\psi = 1$ in each case), but each with its individual actuation capability. The comparison is shown in Figure 9, in the same format as the previous graphs with nondimensional twist curvature versus thickness ratio. Values of the actuator parameters are summarized in the figure.

The figure exemplifies the rather different characteristics of each actuator. For thin substrates ($T \rightarrow 0$), the IDE and UDA actuators provide very high levels of twist, while the PFC and DAP elements are unable to produce much twist due to their dependence on the substrate to induce transverse stress loads. Slightly thicker substrate materials result in a dramatic drop in twist for the IDE and UDA actuators, while the PFC and DAP elements provide twist that reaches a peak at approximately $T = 0.5$. Medium size substrates ($1 < T < 5$) will have the most twist when IDE actuators are incorporated, although the differences in twist become less apparent between the four types. Finally, as the substrate reaches larger thicknesses ($T > 10$), the twist approaches zero for all actuators. The differences in actuators at this point ($T \sim 10$) can be attributed to the different actuation capabilities (Λ_{ACT}), and to the fact that the UDA twist approaches zero as $1/T$, while the other three approach zero as $1/T^2$.

MANUFACTURING AND EXPERIMENTAL RESULTS

Manufacturing of the piezoelectric fiber composite followed procedures given in Reference [11], with the exception that the composite was cured under a pressure of 80 psi in an autoclave curing system. A 15 mm by 94 mm strip was laid up by hand, using 170 μm fibers oriented at 45 degrees. After curing, the composite was lightly sanded and electroded with air-dried silver paint. The composite was poled with an electric field of 25 kV/cm for 20 minutes while in silicon oil at approximately 23°C. Prior to any further steps, the composite was aged for 72 hours to eliminate the possibility of any time-dependent polarization effects.

Properties of the composite were predicted using the Closed Form Combination Model derived in Reference [11]. The width (X_2) and the thickness (X_3) line fractions measured after manufacture were 0.78 and 0.84, respectively. The capacitance was measured and the dielectric constant was found to be 154. From this dielectric constant, and the measured value for X_2, it is possible to calculate an averaged value for X_3, and use this to calculate all the composite properties. This is the single most accurate method to evaluate the through-thickness line fraction (X_3). Small nonuniformities in thickness, sanding and fiber waviness, and the limitations on measurement accuracy make it virtually impossible to measure the true X_3 for a mono-fiber layer composite. The properties are summarized in Table 2.

Once the material properties were characterized, the laminate could be assembled. The composite was cut into two pieces, each of which were bonded to a 0.025 mm (1 mil) stainless steel substrate, with the poling directions oriented outward. The plies were bonded to the steel substrate using an epoxy adhesive (Young's Modulus of 2.8 GPA) and cured at room temperature to avoid possible depolarization. The resulting bond layers measured approximately 0.01 mm (<0.5 mil).

Table 2. Manufactured laminate properties.

Measured				
	X_2	X_3	$\epsilon^T_{33}/\epsilon_0$	
	0.78	0.84	154	
Calculated				
X_3	$R_c = c^E_{22}/c^E_{11}$	$R_d = d_{32}/d_{31}$	$\psi = c_{11}/c^E_{11}$	T
0.86	0.337	0.794	3.67	0.125

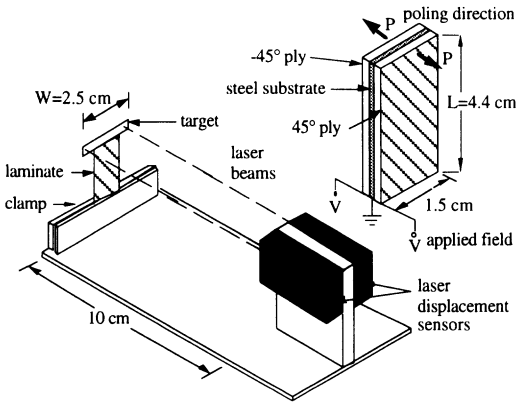

Figure 10. *Experimental set-up for PFC laminate.*

The experimental setup is shown in Figure 10. The $[45_A/0_S/-45_A]$ laminate was clamped at its base, and fitted with a laser target. The active plies were actuated quasi-statically (0.005 Hz) to eliminate the majority of viscoelastic effects that may have been present from the matrix material. Actuation was in-phase, with a 100 volt peak-to-peak (0.5 kV/cm) triangular waveform. Tip displacements were measured using two laser displacement sensors, whose differential outputs provided twist information, and average outputs provided bending information. Using this information and the laminate dimensions, the resulting twist and bending curvatures were calculated:

$$\varkappa_6 = 2\varkappa_{12} = \frac{2(D_1 - D_2)}{LW} \qquad \varkappa_1 = \frac{(D_1 + D_2)/2}{L^2} \tag{26}$$

where D_1 and D_2 are the laser displacements, and L and W are the active length and width shown in Figure 10. Comparison of the experimental curvature strains with the CLPT model is given in Figure 11, where a single entire loop is shown. Excellent agreement is seen for both curvatures. The small magnitude of $\varkappa_1$ shows that almost pure twist actuation was obtained. Deviation from the model is observed at higher field levels, as nonlinear effects become more important.

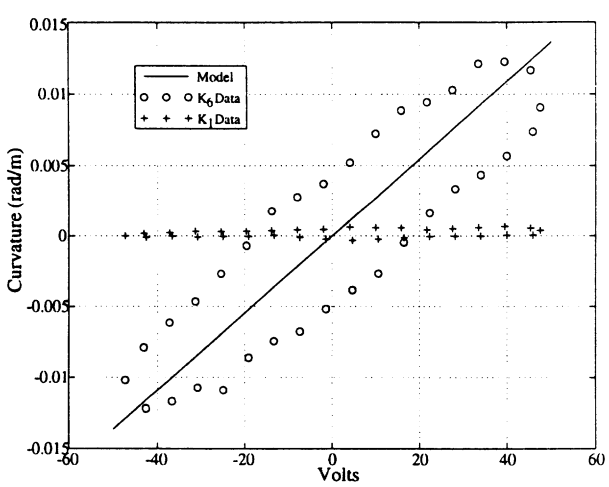

Figure 11. *Comparison of data with model.*

CONCLUSIONS AND FUTURE WORK

This paper presented an investigation into the actuation of laminated structures with anisotropic active materials. The origins of actuator anisotropy, stemming from different in-plane stiffness or actuation properties, contribute to an actuator's ability to induce unequal stress loads. The presence of this anisotropy in actuators enables shear stress to be induced for ply orientations not aligned with the principal ply axes. The incorporation of several active plies into laminated structures introduces the possibility of twist deformation in isotropic substructures. Laminated structures were easily and effectively modeled using an augmented Classical Laminated Plate Theory which includes actuator induced-stress terms.

A twist-extension coupled, antisymmetric laminate was chosen as an example for the study of induced twist. Induced twist was described as a function of structure thickness and actuator material anisotropies. Comparison of four separate actuators highlighted the fundamental difference between stiffness anisotropy and free-strain anisotropy effects. Actuators that have a relatively low transverse stiffness, such as PFC and DAP elements, are unable to induce large transverse loads without a substrate material to provide the structural stiffness. Optimizing the twist actuation requires a particular substrate-to-actuator thickness ratio. Actuators that have high transverse stiffness, such as the IDE and UDA, do not require substrate materials to induce high levels of twist. High levels of free-strain anistropy enhance the twist actuation in these cases. Actuators that have very high stiffness anisotropy, such as DAP elements, would not benefit from added free-strain anisotropy. PFCs have the additional freedom of tailoring material geometry so that the optimum levels of anisotropy may be used for a particular set of material properties.

In order to demonstrate twist actuation in isotropic substrates, a $[45_A/0_S/-45_A]$ laminate was manufactured and tested. This laminate incorporated PFC actuators to induce the actuation loads. Excellent agreement was found between the experimental response and the response predicted through the CLPT model. The results show the feasibility of modeling PFC laminates with laminated plate theory, and further demonstrates the opportunities for anisotropic actuation using this new type of actuator.

Future work will continue to improve piezoelectric fiber composite actuators. The present work has shown that high twist actuation can be achieved in thin structures with transversely stiff actuators, whereas high actuation capabili-

ties discern the actuators used with thicker structures. Interdigitated electrode piezoceramics have these characteristics and demonstrate good twist actuation throughout the range of structure sizes. However, issues of conformability, reliability, and the benefit of tailoring still point to piezoelectric fiber composites as an attractive alternative to monolithic ceramics. The next step will be to combine these two technologies. The use of etched copper/Kapton electrodes will permit interdigitated electrodes on piezoelectric fiber composites. This new approach, in conjunction with improved matrix material properties, has the potential to make piezoelectric fiber composite actuators extremely advantageous for structural control applications.

ACKNOWLEDGEMENTS

This work was supported by a grant from the Office of Naval Research (#N00-14-92-J-4067).

APPENDIX

The plane stress constitutive constants may be expressed in terms of the full 3-dimensional constants as follows:

$$c_{11}^{E*} = c_{11}^{E} - \frac{c_{13}^{E^2}}{c_{33}^{E}} \qquad c_{12}^{E*} = c_{12}^{E} - \frac{c_{13}^{E} c_{23}^{E}}{c_{33}^{E}}$$

$$c_{22}^{E*} = c_{22}^{E} - \frac{c_{23}^{E^2}}{c_{33}^{E}} \qquad c_{66}^{E*} = c_{66}^{E} \qquad e_{31}^{*} = e_{31} - \frac{c_{13}^{E} e_{33}}{c_{33}^{E}}$$

$$e_{32}^{*} = e_{32} - \frac{c_{23}^{E} e_{33}}{c_{33}^{E}} \qquad \epsilon_{33}^{S*} = \epsilon_{33}^{S} + \frac{e_{33}^{2}}{c_{33}^{E}} \tag{27}$$

REFERENCES

1. Crawley, E. F. and E. H. Anderson. 1990. "Detailed Models of Piezoceramic Actuation of Beams", *Journal of Intelligent Material Systems and Structures*, 1:4–25.
2. Crawley, E. F. and K. Lazarus. 1991. "Induced Strain Actuation of Isotropic and Anisotropic Plates", *AIAA Journal*, 29(6):944–951.
3. Jia, J. and C. A. Rogers. 1989. "Formulation of a Laminated Shell Theory Incorporating Embedded Distributed Actuators", *Adaptive Structures, A-D Vol. 15* B. K. Wada, ed., NY: ASME.
4. Hagood, N. W., W. H. Chung and A. H. von Flotow. 1990. "Modeling of Piezoelectric Actuator Dynamics for Active Structural Control", *Journal of Intelligent Material Systems and Structures*, 1(3):327–354.
5. Lazarus, K. and E. F. Crawley. 1992. "Multivariate High-Authority Control of Plate-Like Active Structures", AIAA Paper No. 92-2529, *Proceedings of the 33rd AIAA Conference on Structures, Structural Dynamics, and Materials*, Dallas, TX.
6. Rogers, C. A. and C. R. Fuller. 1991. "Recent Advances in Active Control of Sound and Vibration", *Proceedings of the VPI and SU Conference on Recent Advances in Active Control of Sound and Vibration*, Blacksburg, VA.
7. Barrett, R. M. 1993. "Modeling Techniques and Design Principles of a Low Aspect Ratio Active Aeroservoelastic Wing", Paper No. 1917-10, *Proceedings of the 1993 North American Conference on Smart Structures and Materials*, Albuquerque, NM.
8. Ehlers, S. M. and T. A. Weisshaar. 1992. "Effect of Adaptive Material Properties on Static Aeroelastic Control", AIAA Paper No. 92-2526, *Proceedings of the 33rd AIAA Structures, Structural Dynamics, and Materials Conference*, Dallas, TX.
9. Skinner, D. P., R. E. Newnham and L. E. Cross. 1978. "Flexible Composite Transducers", *Material Research Bulletin*, 13:599–607.
10. Smith, W. A. and B. A. Auld. 1990. "Modeling 1-3 Composite Piezoelectrics: Thickness-Mode Oscillations", *IEEE Transactions on Ultrasonics, and Frequency Control.*
11. Hagood, N. W. and A. A. Bent. 1993. "Development of Piezoelectric Fiber Composites for Structural Actuation", AIAA Paper No. 93-1717, *Proceedings of the 34th AIAA Structures, Structural Dynamics, and Materials Conference*, La Jolla, CA.
12. IEEE Std 176-1798. 1978. *IEEE Standard on Piezoelectricity.* The Institute of Electrical and Electronics Engineers.
13. Hagood, N. W., R. Kindel, K. Ghandi and P. Gaudenzi. 1993. "Improving Transverse Actuation of Piezoceramics Using Interdigitated Surface Electrodes", SPIE Paper No. 1917-25, *Proceedings of the 1993 North American Conference on Smart Structures and Materials*, Albuquerque, NM.
14. Jones, R. M. 1975. *Mechanics of Composite Materials.* New York: Hemisphere Publishing Corp.